Received: 8 October 2023 | Revised: 12 December 2023 | Accepted: 15 December 2023 | Published online: 20 December 2023

RESEARCH ARTICLE

Artificial Intelligence and Applications
2024, Vol. 2(3) 204–217
DOI: 10.47852/bonviewAIA32021848

BON VIEW PUBLISHING

Epilepsy Detection by Different Modalities with the Use of AI-Assisted Models

Jayanthi Vajiram[1,*], Sivakumar S.[1], Roanek Jena[1] and Utkarsh Maurya[1]

[1]*Vellore Institute of Technology, India*

Abstract: Epilepsy is characterized by recurrent seizures originating from any four brain lobes. It includes focal seizures with symptoms of alterations in consciousness and cognitive impairments, including memory and language difficulties. It must be radiologically identified by proper diagnosis and course of therapy. However, a visual inspection of images may not always yield an accurate interpretation from radiologists, necessitating AI-assisted methods. The computer-vision-based radiological methods are used to enhance the treatment of epilepsy by image bio-markers and deep learning algorithms. These methods are used to predict disease progression and treatment. It specifies the focus of the research on epilepsy detection using new U-transfer reinforced Gaussian network (U-TRGN) classification models. These models used for lateralization and localization of brain activity in this process. This study gives the idea of preoperative findings of different imaging modalities and postoperative findings of Electroencephalography (EEG) data analysis. The data have been pre-processed through normalization, smoothing, and noise removal techniques. The data are then classified using U-TRGN, after feature selection by kernel convolutional analysis. The performance metrics are evaluated through the training accuracy, validation accuracy, precision, dice coefficient, and area under a region of the convergence curve. The proposed technique attained an accuracy of 97.04%, precision of 94.12%, dice coefficient of 2.96%, and AUC of 99.56%, which is better than the existing methods, and it will be a baseline for upcoming studies.

Keywords: epilepsy, new U-TRGN model, KCA algorithm, deep learning models

1. Introduction

The epilepsy is a neurological disorder and a non-communicable disease [1]. The abnormality occurs, when the electrical activity of brain disrupts a part or entire body with sudden seizures. Around 60 million people worldwide suffer from a variety of epileptic seizures. These epilepsies affect static memory and cognitive abilities that can make serious brain injury to the patient. The patient experiences trouble in normal communication with society, which leads to the humiliation and absence of fitting societal position. They are treated by different modalities and also by using MRI-guided stereotactic laser interstitial thermal therapy [2]. Thus, early recognition of epileptic seizures can help patients to lead quality life. Treatment procedures are carried by checking the neuroimaging modalities and case history [3, 4]. EEG data can provide valuable insights into the lateralization and localization of brain activity of the patients. Lateralization shows either the left or right hemisphere of the brain activities. In the context of epilepsy detection, lateralization can help determine which hemisphere of the brain is primarily affected by abnormal electrical activity. Localization refers to the specific brain regions or areas that are involved in epileptic seizures. The various diagnostic tests include electrocorticography (ECoG), magnetoencephalography, positron emission tomography (PET), single-photon emission computed tomography, functional MRI (fMRI), and functional near-infrared spectroscopy methods [5]. The abnormalities are widespread throughout the brain, and to identify the brain region by manual annotation of individual scans gives 5–10% error. The 86% of affected cases were overlooked, according to the earlier study [6]. For instance, one-third of healthy adults have unilaterally enlarged temporal horns and aberrant hippocampal signaling visible on fluid-attenuated inversion recovery (Flair) and T2-weighted imaging. Convolutional neural networks (CNNs) are a group of profound learning method, which gives better execution of features and characters in the dataset. A machine learning (ML) classifier of support vector machine (SVM), deep belief network (DBN), k-nearest neighbor (KNN), random forest (RF), deep neural network (DNN), and U-transfer-reinforced Gaussian network (U-TRGN) could be used to solve this issue. The classifier models have a bunch of processing methods, and the results of detecting epilepsy support to minimize the medical procedure. The classification models, which give hidden or obscure factors in data, may provide more accurate outcomes compared to the old statistical methods [7]. The postoperative seizure control imaging investigations offer predictions of individual patient outcomes and relationship across entire cohorts and give significant advancement in personalized patient care. This study explains the classification models used to detect abnormal brain activity patterns through lateralization and localization information and achieve higher accuracy in detecting and localizing epileptic seizures.

2. Literature Review

The cognitive deterioration can occur in 70–80% of cases, and this is influenced by various epilepsy-related features [8]. Long-term epilepsy-associated tumors are typically low-grade, slowly growing

*Corresponding author: Jayanthi Vajiram, Vellore Institute of Technology, India. Email: jayanthi.2020@vitstudent.ac.in

tumors located in the cortex, and they primarily affect young patients with family medical histories of epilepsy [9]. Epilepsy gives noticeable effects on behavior and cognitive abilities. Evidence proves that epilepsy can also impact behavior as observed through structured interviews assessing through five-factor model of personality test [10]. Studies of epilepsy proved with sleep disturbances using the trail making test [11]. Correlations between changes in neuropsychological test scores and brain metabolism have been explored using statistical parametric mapping, which indicates metabolic changes by the Boston Naming Test [12]. Volumetric MRI identifies epilepsy progression of brain atrophy [13]. The single-voxel spectroscopy has been used to compare children with different seizure types and to differentiate patients with intractable and non-intractable epilepsy [14]. To diagnose and categorize the epilepsy, ML techniques give effective analysis of discriminative characteristics generated from brain pictures, with SVMs classifiers on the MRI data [15] and diffusion tensor imaging (DTI) data of individuals with mesial temporal lobe epilepsy [16]. Quantitative relaxometry and DTI data were used with SVM [17] to enhance the identification of temporal lobe epilepsy. The CNN classifier is used for histopathological assessment of WSI images to recognize different subtypes of focal cortical dysplasia with hyperplasia in epilepsy cases [18]. The nocturnal frontal lobe epilepsy was analyzed with two-dimensional self-organizing maps, which are used to cluster the data into seizure and non-seizure patterns [19]. The XAI4EEG system of data under time constraints significantly reduced the time needed to validate predictions and improved interpretability compared to SHAP feature contribution plots [20]. The SVM classifier detects epileptic seizures in long-term EEG data [21]. EEG signals offer a solution for seizure prevention by classification performance scores of accuracies, Area Under the receiver operating characteristic curve AUC-ROC curve, sensitivity, and specificity [22]. The signal was analyzed to extract features for a classifier detecting activation and quiescent phases. The classifier's output was then applied to a finite state machine for cyclic alternating pattern method. The classifiers were tested using a sequential feature selection algorithm and principal component analysis [23]. The two decision forest classifiers, SysFor and Forest CERN, were applied to an ECoG brain dataset. The results showed that these classifiers significantly reduced seizure detection time while maintaining high accuracy. Additionally, they were able to identify the specific region of the brain most affected by seizures. FCM (fuzzy c-mean) and SVM methods were used to create an image segmentation method by combining the two preceding algorithms and testing its efficacy in a brain image with high bias and noise. Ontology-based heterogeneous feature detection with classifiers models also gives better results. The dataset from Temple University School of Medicine analyzed by six pre-trained models, namely Alex Net, GoogLeNet, Inception-v3, ResNet18, VGG16, and VGG19, was used for seizure classifications [24, 25]. Deep Convolutional Neural Network (DCLNN) model was used to analyze the resection cavities on postsurgical epilepsy patient dataset [26]. Diffusion kurtosis tensor was used to identify the epilepsy [27]. A comprehensive analysis of 190 studies revealed a growing preference for using CNNs along with time-frequency decomposition method images. EEG signals with their subjective interpretation can sometimes result in misdiagnosis. To address this issue, this research paper introduces a deep learning model for seizure detection. The model employs a two-dimensional representation of EEG features and exhibits excellent scalability in neural networks. It demonstrates high applicability and accuracy in classifying seizures [28–31]. Microglial TRPV1 has been found to have a role in neuroinflammatory reactions, associated with seizures. Researchers have proposed a Takagi–Sugeno–Kang fuzzy system framework to classify epilepsy data, which can aid the treatment planning. Algorithm called MVTL-LSR, based on multi-view transfer learning, has been proposed to study epileptic EEG signals and enhance AI-assisted recognition of epilepsy. The SECNN-LSTM algorithm has shown effectiveness in predicting EEG signals related to epilepsy, leading to improved recognition rates for the disease. The prompt removal of artifacts from EEG signals is crucial to preserve the original signal features and ensure robust classification for accurate epilepsy detection by Google Net, VGG16, and Alex Net models with k-fold cross-validation. The earlier study used the OAOFS-DBNECD technique, which transformed the signals into a.csv format. For the design of the epilepsy EEG analysis model, an auto ML algorithm was utilized, which automatically generated a model based on the input data [32–41].

2.1. Theoretical framework

2.1.1. Imaging modalities used in epilepsy cases

The epilepsy studies were analyzed at the Cerebrum Imaging Centre using preoperative MRI data. This suggests that the center is using MRI scans to study epilepsy cases before the patients undergo surgery. This type of study can help identify abnormalities or specific regions in the brain that contribute to epileptic seizures.

The data acquisition and imaging setup were used at the Imaging Center. This included 3 T Siemens Magnetom Prisma-Fit furnished with a 64-channel head curl. Following a T1-weighted (T1w) structural scan, participants underwent resting-state fMRI (rs-fMRI) and multi-shell diffusion-weighted imaging (DWI). In addition, two spin-echo images were taken to correct individual rs-fMRI scan distortion. Two T1w checks with indistinguishable boundaries were obtained with a 3D charge arranged fast inclination reverberation succession (MP-fury; 0.8 mm isotropic voxels, lattice = 320 × 320, 224 sagittal cuts, (repetition time) TR = 2300 ms, (echo time) TE = 3.14 ms, TI = 900 ms, flip point = 9°, iPAT = 2, halfway Fourier = 6/8). Before being submitted for further processing, both T1w scans were visually examined to ensure that there was minimal head movement. qT1 relaxometry information was gained utilizing a 3D-MP2RAGE grouping (0.8 mm isotropic voxels, 240 sagittal cuts, TR = 5000 ms, TE = 2.9 ms, TI 1 = 940 ms, T1 2 = 2830 ms, flip point 1 = 4°, flip point 2 = 5°, iPAT = 3, data transfer capacity = 270 Hz/px, reverberation dividing = 7.2 ms, halfway Fourier = 6/8). We joined two reversal pictures for qT1 planning to limit aversion to B1 inhomogeneities and improve intra- and between-subject reliability. To obtain DWI data, a 2D spin-echo echo-planar imaging sequence with multi-band acceleration was used. The image sequence consisted of three shells with b-values of 300, 700, and 2000 s/mm^2 and 10, 40, and 90 diffusion weighting directions per shell********* 1.6 mm isotropic voxels, TR = 3500 ms, TE = 64.40 ms, flip angle = 90°, refocusing flip angle = 180°, FOV = b0 pictures obtained backward stage encoding bearing are likewise accommodated mutilation adjustment of DWI examines. One 7 min rs-fMRI examine was gained utilizing multiband sped up 2D-intense reverberation planar imaging (3 mm isotropic voxels, TR = 600 ms, TE = 30 ms, flip point = 52°, FOV = 240 × 240 mm^2, cut thickness = 3 mm, mb factor = 6, reverberation separating = 0.54 ms). Members were told to keep their eyes open, take a gander at an obsession cross, and not nod

Figure 1

Different imaging modalities were used to map hypometabolism in epilepsy patients before surgery. This included (A) magnetic resonance imaging (MRI) and (B) post-operative X-ray images. (C) Preoperative and postoperative MRIs were segmented and subtracted (shown in red) to determine the volume of removed tissue. (D) MRI registration was done for FDG-PET imaging to assess hypometabolism. (E) Comparison of hypometabolism was made with healthy controls (shown in green). (F) The resection area overlaid with hypometabolism (highlighted in green-light green) helped determine the extent of resected hypometabolism profiles

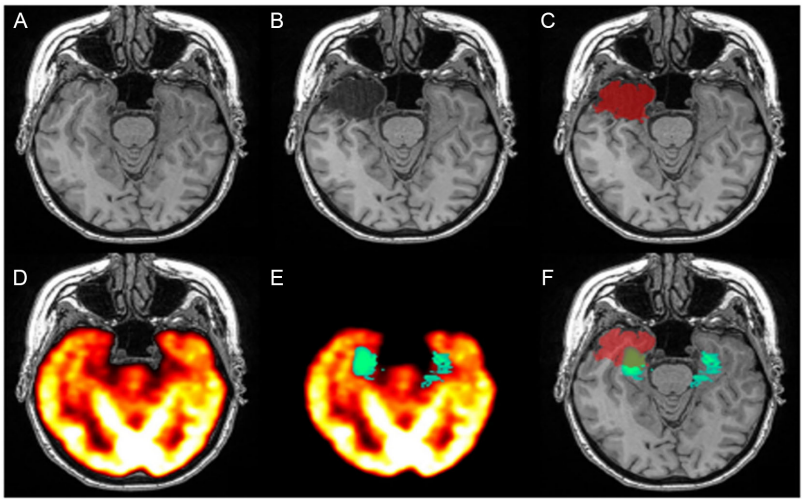

off. To correct for distortion in the rs-fMRI scans, we also include two spin-echo images encoded in reverse phase (TR = 4029 ms, TE = 48 ms, flip angle = 90°, FOV = 240 240 mm^2, echo spacing = 0.54 ms, phase encoding = AP/PA, bandwidth = 2084 Hz/Px). The timing difference between slices was adjusted after the scans were checked for significant head movement (more than 3 mm or 3°). The images were realigned to the middle slice after being spatially normalized to the MNI template. The automated anatomical labeling atlas (23), used to segment the brain into 116 regions, includes 90 regions in the cerebrum and 26 regions in the cerebellum. These region of interest (ROIs) were used as nodes in the construction of the resting-state functional network. The comprehensive imaging protocol that comes with this data release contains the number of parameters used in the acquisition are clearly explained in Figure 1.

Fluoro-deoxyglucose positron emission tomography (FDP-PET) imaging set up for Epilepsy detection typically use the radiotracer, is a radioactive form of glucose that is injected into the patient's bloodstream, tracer travels through the body and is taken up by brain active cells of higher glucose metabolism, than scanning, imaging and analysis was captured.

2.1.2. Isotopes used in PET scans

Table 1 shows the isotopes used in the PET scans. X-ray and CT scanning parameters give the slice thickness, scan range, and radiation dose and acquire a series of 2D images in axial, coronal, or sagittal planes. The X-ray beam rotates around the patient; capturing multiple images from different angles scan gives the detailed anatomical images of the brain, they may not always be sufficient for detecting certain types of epileptic activity. Additional imaging modalities with EEG are required in initial stage of epilepsy detection. CT scans help to identify epilepsy-related abnormalities or other brain lesions by very low range of 7–10% proved by NIH studies. Cyclin-dependent kinase-like 5 (CDKL5) genetic variation that leads to the development of epileptic encephalopathy was recognized on 2004 as shown in Figure 2.

EEG mainly used for the early stage and surgical stage of epilepsy detection. In cases where medications fail to adequately control seizures, it leads to surgery. EEG is used to precisely locate the seizure foci or the specific area in the brain responsible for generating seizures. This helps to perform surgical procedures to remove or disconnect the seizure focus. The different imaging modalities help to compare the epilepsy symptoms and surgical intervention.

Table 1
Isotopes used in PET scans

Isotype	^{11}C	^{13}N	^{15}O	^{18}F	^{68}Ga	^{64}Cu	^{52}Mn	^{55}Co	^{9}Zr	^{82}Rb
Half-life	20 min	10 min	2 min	110 min	67.81 min	12.7 h	5.6 day	17.5 h	78.4 h	1.3 min

Figure 2
The genetic variant leads to epilepsy

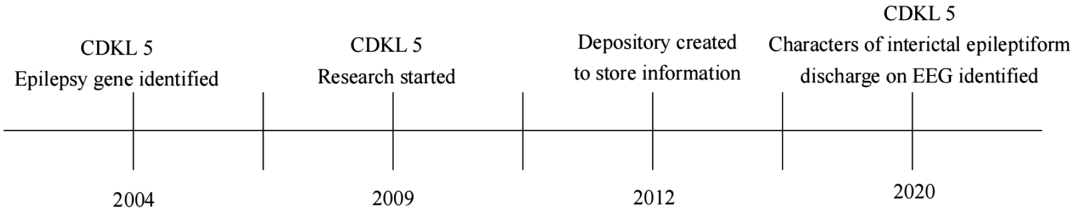

Figure 3
The system model of epilepsy classification and detection

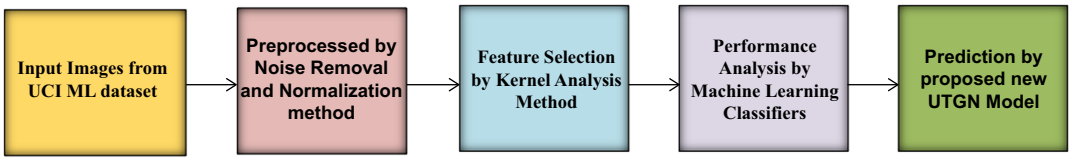

3. Research Methodology

3.1. Dataset details

The original dataset consists of 500 individuals, each with 4097 data points representing brain activity recorded over 23.6 s. The data are divided into 23 chunks, with each chunk containing 178 data points for 1 s. The last column of each chunk represents the label, with values ranging from 1 to 5 representing different conditions. The dataset has the captured image on 5 ways or class like eyes open, eyes closed, healthy brain area, area with a tumor and area with seizure activity. Class 1 represents recordings of seizure activity, while classes 2–5 represent non-seizure conditions (eyes open, eyes closed, healthy brain area, and area with a tumor).

The input vector {1, 2, 3, 4, 5} has a column called "*y*," which represents the categories of the 178-dimensional input vector. This column provides information about the patient's eyes being open or closed, tumor location, and seizure activity. To streamline the multi-classification task, the different classes {2, 3, 4, 5} were grouped as 0, denoting "not epileptic seizure," while class {1} was kept as 1, representing an "epileptic seizure." This approach can also aid in pinpointing the localization and lateralization of brain activity during seizures, offering insights into the specific brain regions implicated in epilepsy. It can also be used to localize and lateralize the brain activity during seizures to better understand the specific regions of the brain involved in epilepsy. This information is valuable for treatment planning of epilepsy.

Figure 3 includes the following components: EEG data acquisition, pre-process to remove artifacts and noise, higher-level features selection based on time domain series, and kernel convolutional analysis (KCA) algorithm was applied to identify the most informative features for epilepsy characteristics. The selected SVM, DBN, KNN, RF, DNN, and KA-U-TRGN classifier models are unique approaches of learning patterns and making epilepsy predictions based on the extracted features. After the parameters are evaluated by model integration and fusion, the final prediction by displaying graphical representations helps for medical intervention.

3.2. Feature selection using kernel analysis (KCA)

In feature selection using kernel analysis (KCA), the mean is computed for each feature in the image by iterating through each feature and then subtracted from each feature vector to eliminate bias and center the data around zero. The covariance matrix is used to measure the relationship between different features in the dataset. The eigenvalue decomposition is performed to find the eigenvectors and eigenvalues of the covariance matrix. The eigenvectors represent the directions in which the data vary the most, while the eigenvalues correspond to the variance. The top k eigenvectors are selected corresponding to the largest eigenvalues. These eigenvectors capture the most important features and can be used for dimensionality reduction. The dataset is projected onto the selected eigenvectors to obtain the reduced dimensional representation. This can be done by taking the dot product of the centered dataset and the selected eigenvectors. To obtain the reconstructed data from original dataset, first need to multiply the selected eigenvectors by the corresponding eigenvalues and then add back the mean value that was subtracted during PCA (principal component analysis) transformation. This reconstructed dataset represents the original dataset in a reduced feature space. By reducing the dimensionality, improves the efficiency and effectiveness of the model. Finally, the performance of the feature selection is evaluated using a performance metric of choice, such as classification accuracy or mean squared error. The selected features can be used for further analysis or modeling tasks.

Assuming a dataset C with dimensions N and d, we first get sample mean mj of the j-th feature as Equation (1).

$$m_j = \frac{1}{N}\sum_{i=1}^{N} C(i,j) \tag{1}$$

Following that, we determine zero-mean dataset B as Equation (2).

$$B = C - em^T \tag{2}$$

In this case, e stands for a N by 1 vector containing only ones. The Z covariance matrix is constructed in the third step as shown in Equation (3).

$$Z = \frac{B^* B}{N-1} \tag{3}$$

Fourth, the eigendecomposition expression for the covariance matrix Z is given by Equation (4).

$$Z = XYX^{-1} \tag{4}$$

Here, Y stands for eigenvalue matrix, which is also a diagonal matrix, and X stands for the eigenvector matrix given in Equation (5).

$$Y = \begin{bmatrix} Y(1,1) & & & \\ & Y(2,2) & & \\ & & \ddots & \\ & & & Y(d,d) \end{bmatrix} \tag{5}$$

Fifth, X and Y are rearranged to make the eigenvalue decrease as shown in Equation (6).

$$Y(1,1) \geq Y(2,2) \geq \cdots \geq Y(d,d) \tag{6}$$

The sixth step is to determine the total variance for each eigenvector by Equation (7).

$$G(k) = \sum_{i=1}^{k} Y(i,i)$$

$$G = [G(1)G(2)\cdots G(d)] \tag{7}$$

Seventh, assuming T to be the threshold, we choose L* to satisfy given in Equation (8).

$$L^* = \arg\min\left\{L \mid \frac{G(L)}{G(d)} \geq T\right\} \tag{8}$$

The most crucial principal component for L was produced. Kernel PCA (KPCA), a potent PCA version, has been presented by researchers as a solution to this issue. The KPCA uses the identical implementation as PCA with the exception of moving dataset C into a higher-dimensional space. There were two KPCAs examined. Polynomial kernel PCA (PKPCA), for example, is defined as Equation (9).

$$k(x, y \mid \text{PKPCA}) = [a(x \times y) + b]^c \tag{9}$$

where a, b, and c are the kernel parameters. RBF kernel PCA (RKPCA) is the alternative given by Equation (10).

$$k(x, y \mid \text{RKPCA}) = \exp\left(-\frac{||x - y||^2}{d^2}\right) \tag{10}$$

where d represents the scaling factor. In this section, CNN parameters, layers, and structure are discussed. A CNN typically consists of three main layers: convolutional, pooling, and fully connected. It convolves the input image to make different component maps, and the network goes through two stages of training. In feed-forward step, input images are taken, each neuron's input and parameters are combined using a dot product, and a convolution operator is used in each layer. Network output is compared to desired output utilizing a loss function and error rate before back propagation stage, which begins with error. This is repeated for a sufficient number of images. In order to preserve the same output size, zero-padding is applied to the input data. This is done consistently across all the convolutional layers in this study. By adding zeros to the information framework, the resulting grid size 4 × 4 remains unchanged. This ensures consistency in the structure of the neural network and supports image processing.

Initialization of weight: Network convergence can be accelerated with the right initial weights. The literature has presented a variety of weight initialization strategies. After examining the effects of various initializers, this study found that the "He" initializer with a normal distribution provides the best performance.

Function of activation: For the most part, a nonlinear administrator or enactment capability is utilized in profound establishments after convolutions. Presence of this capability model in correlation with a direct method is given in Equation (11).

$$\text{relu}\,(x) = \begin{cases} x & \text{if } x \geq 0 \\ 0 & \text{if } x < 0 \end{cases} \tag{11}$$

Leaky ReLU, as stated in Equation (12), has frequently outperformed ReLU. When the function is not in use, it permits a tiny, non-zero gradient.

$$\text{leaky}_{\text{ReLU}\,(x)} = \begin{cases} x & \text{if } x \geq 0 \\ ax & \text{if } x < 0 \end{cases} \tag{12}$$

A = typically 0.3. The accuracy of classification and training speed have been improved by exponential linear units (ELUs). ELU accepts negative values, which enables it to more efficiently normalize mean unit activations toward zero than batch normalization as shown in Equation (13).

$$\text{ELU(x)} = \begin{cases} \text{x} & \text{if x} \geq 0 \\ \text{a}(\text{e}^{\text{x}} - 1) & \text{if x} < 0 \end{cases} \tag{13}$$

$a = 1$. Additionally, the effectiveness of the developing networks is evaluated when scaled exponential linear unit (SELU) activation function is present. The SELU is created by giving the ELU a little twist. Given below in Equation (14) are the equivalent equations for these functions, with $a = 1.6732$ and $l = 1.0507$.

$$\text{SELU}(x) = \lambda \begin{cases} x & \text{if } x \geq 0 \\ ae^x - \alpha & \text{if } x < 0 \end{cases} \tag{14}$$

Pooling: When a convolutional layer is followed by a pooling layer, size of feature maps and number of parameters in network are reduced, resulting in lower computational costs. Because of adjoining pixels in computations, pooling layers are invariant to little changes. Max-pooling is one of the most widely utilized pooling strategies.

Regularization: Creation of a method that is effective not only with training data but also with new entries is the primary challenge in ML. For deep learning, a number of regularization strategies have been proposed. Dropout, a powerful but cost-effective computational regularization technique, is used in this paper. During the training phase, it randomly removes some of fully connected layer's nodes to prevent over-fitting. Then again, dropout is considered as a group technique, since it gives various organizations during preparing.

Dietary function: The choice of loss function that should be minimized is one of the most crucial aspects of designing a DNN. Typically, the categorical cross-entropy function (H), which was used in this case, is shown in Equation (15).

$$H(p, q) = -\sum_x p(x)\ln(q(x)) \tag{15}$$

Algorithm of KCCA

INPUT: Dataset
RESULT: The identification of neurological disorders is based on a number of factors.
Load the brain image dataset in the proposed model
Pre-processing is used to remove undesined noise from a dataset.
Select features of pre-processed image
for each epoch in epoch Number do
for each bunch in balchised do
y′= model(feanires).
loss = crossEntropy (y, y′)
whilet < Maximum number of iterations)
Adjust the revitalization velocities and positions to come up with new solutions.
if $r > s_y$)
At randiam, choose a solution from the best solutions.
Create a local solution that is close to the best-selected option.
end if
if $r < b_i$ & $f(x_i) < f$(Gbest))
Increase s_i and decrease b_i
end if
Rate the hats and identify the current Gbest
end while
acco:
b^* *Acc* = max(b^* *Acc*, *acc*);
Return

A CNN typically consists of three main layers: convolutional, pooling, and fully connected. It convolves the input image to make different component maps, and the network goes through two stages of training. In feed-forward step, input images are taken, each neuron's input and parameters are combined using a dot product, and a convolution operator is used in each layer. Network output is compared to desired output utilizing a loss function and error rate before back propagation stage, which begins with error. This is repeated for a sufficient number of images. In order to preserve the same output size, zero-padding is applied to the input data. This is done consistently across all the convolutional layers in this study. By adding zeros to the information framework, the resulting grid size 4 × 4 remains unchanged. This ensures consistency in the structure of the neural network and supports image processing.

3.3. Classification using proposed U-TRGN

A fully connected CNN called U-Net is used for effective semantic segmentation. The U-Net DNN can be used for a wide range of analytical tasks. This is especially helpful in medical imaging. The U-Net design depends on an auto-encoder network, and it will duplicate its contributions to its results. U-Net contains two ways, a compression way (encoder) and a symmetric growing way (decoder). Transposed convolutions are used in the decoder path, allowing for precise localization. U-Net was initially intended for 572 × 572 pixels; it very well may be effectively altered to work with any image aspect. A few stacked convolutional layers are highlighted from the images, as shown in Figure 3.

In this approach, the U-TRGN are used for classification. The U-TRGN model is a combination of transfer learning and reinforcement learning (RL) techniques. First, the model used to extract features from the data. Next, the model applies a feature selection technique KCA to select the most relevant features from the UNet model output. KCCA is a statistical method that finds linear combinations of variables that have maximum correlation with the target variable. Once the features are selected, the U-TRGN model is trained and provides an effective way to classify data by extracting relevant features using the UNet model, selecting the most informative features through KCA, and optimizing the classifier model. This approach combines the strengths of transfer learning, and feature selection, to achieve accurate and efficient classification of data as explained in Figure 4.

The efficient algorithm makes RL possible. The classification challenge necessitates the sequential decision-making. The algorithm of a multi-featured approach and a multilayer perceptron neural network is used in this study. The class labels of image are converted into source vector representation. The reward function depends on the state and action rather than the class. In each RL formulation, the agent is an intuitive but formalized concept that acts in different states and receives specific rewards. The recommended set of actions that maximizes the overall expected cumulative reward received. Consequently, the ideal strategy for the specialist to follow. This scenario is defined by an image volume and a scalar number that shows whether prior class prediction (epilepsy vs. normal) was accurate. This prediction's accuracy is shown by pred_corr. It is described by Equation (16).

$$\text{pred\_corr} = \begin{cases} 1, & \text{if prediction is correct} \\ 0, & \text{if prediction is wrong.} \end{cases}$$

$$\text{pred\_corr} \equiv \delta_{a,l_{\text{KC}}} \tag{16}$$

where δ is the Kronecker delta function given by Equation (17).

$$s = \{\mathcal{M},\ \text{pred\_corr}\}, \tag{17}$$

In order to streamline the 3D convolutional backpropagation process and ensure consistent matrix sizes, the x and y plane of the original images were resized to 64 × 64 pixels. Additionally, to standardize the depth dimension, extra slices of 64 × 64 pixels were added to the bottom of the images with varying numbers of cuts (ranging from 28 to 36). This adjustment ensured that all images had a uniform z-axis length of 36 tomahawks. In essence, this is padding in z-direction. Two possible actions, a1 and a2, are simply prediction of whether image M is normal or epilepsy containing as shown in Equation (18).

$$\mathcal{A} = \begin{pmatrix} a_1 \\ a_2 \end{pmatrix} = \begin{pmatrix} 0 \\ 1 \end{pmatrix} = \begin{pmatrix} \text{predict normal} \\ \text{predict epilepsy} \end{pmatrix} \tag{18}$$

Rewards are given for accurate class predictions: +1 for correct predictions and −1 for incorrect predictions. The reward r can be defined in terms of prediction accuracy, pred_corr by Equation (19).

$$r = \begin{cases} -1, & \text{if pred\_corr} = 0 \\ +1, & \text{if pred\_corr} = 1. \end{cases} \tag{19}$$

In RL, the action-value function, indicated by Q (s, a), is a crucial element. An "episode" is a collection of states where an agent restarts in a different state. Action-value function shows the anticipated cumulative reward if, after doing action, a predetermined process for choosing actions is followed until the end of the episode.

Figure 4
U-TRAN architecture for the image classification model

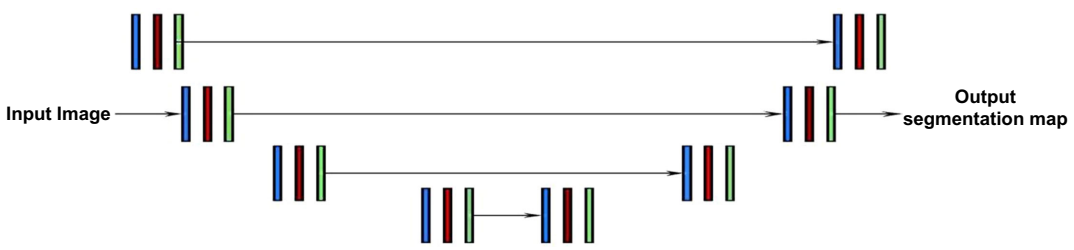

The Q-value represents the expected total reward that will be obtained when taking a specific action in a specific state, based on a given policy is defined by Equation (20).

$$Q^{\pi}(s,a) = E_{\pi}\{R_t \mid s_t = s, a_t = a\} = E_{\pi}\left\{\sum_{k=0}^{\infty} \gamma^k r_{t+k+1} \mid s_t = s, a_t = a\right\} \quad (20)$$

where ERt|st = s, at = an is expectation for Rt upon choosing action an in-state s and subsequently choosing actions in accordance with, and Rt is total cumulative reward commencing at time t. The weighting of "instant gratification" versus "delayed gratification" is represented by the discount factor of 0.99. By maximizing it, the action-value function is crucial and, eventually arriving the desired behavior, leads to an accurate image class prediction. Two-node output depicts the two possible action-values, Q (s, $a1$) and Q (s, $a2$), that can be obtained by acting on state s in either of two different ways as shown in Equation (21).

$$p(x) = \sum_{j=1}^{K} \pi_j p(x;\theta_j),\ j = 1,\ldots,K.$$

$$p(\mathbf{x}) = \sum_{c=1}^{C} \pi_c f_c(\mathbf{x} \mid \theta) \quad (21)$$

Mixture model has a vector of parameters, $\underline{\theta} = \{\theta_1,\ldots,\theta_k,\pi_1,\ldots\pi_k\}$.

Hidden variables are treated as a latent variable, or Z, in mixture models. It accepts numbers 1 through K as a discrete set that satisfies the conditions $z_k \varepsilon \{0,1\}$ and $\sum_z z_k = 1$. A conditional distribution p ($x \mid z$) and a marginal distribution p (z) are how we define the joint distribution p (x, z) given by Equation (22).

$$p(z,x) = p(z)p(x \mid z)$$

$$p(z_k = 1) = \pi_k \quad (22)$$

A definition of probability density function of X is given in Equation (23).

$$p(x \mid \mu_k, \Sigma_k) = \frac{1}{\sqrt{2\pi|\Sigma^{-1}|}} \exp\left(-\frac{1}{2}(x-\mu_x)\Sigma_x^{-1}(x-\mu_x)^T\right)$$

$$f_c(\mathbf{x} \mid \mu_c, \mathbf{\Sigma}_c) = \frac{1}{(2\pi)^{\frac{d}{2}}|\mathbf{\Sigma}_c|^{\frac{1}{2}}} \exp\left(-\frac{1}{2}(\mathbf{x}-\mu_c)^t \mathbf{\Sigma}_c^{-1}(\mathbf{x}-\mu_c)\right) \quad (23)$$

A linear superposition of Gaussians is utilized to represent a Gaussian mixture distribution in the form by Equation (24).

$$p(x) = \sum_{k=1}^{K} \pi_k p(x \mid \mu_k, \Sigma_k)$$

$$\hat{\pi}_c = \frac{n_c}{n},$$

$$\hat{\mu}_c = \frac{1}{n_c} \sum_{\{f|y_i=c\}} \mathbf{x}_i$$

$$\hat{\mathbf{\Sigma}}_c = \frac{1}{(n_c-1)} \sum_{\{i|y,=c\}} (\mathbf{x}_i - \mu_c)(\mathbf{x}_i - \mu_c)^t \quad (24)$$

Given a certain value of z, conditional distribution of x is now a Gaussian by Equation (25).

$$p(x \mid z_k = 1) = p(x \mid \mu_k, \Sigma_k)$$

$$p(x \mid z) = \prod_{k=1}^{K} p(x \mid \mu_k, \Sigma_k)^k \quad (25)$$

By adding joint distribution of all possible states of z, one can obtain the marginal distribution of x given in Equation (26).

$$p(x) = \sum_z p(z)p(x \mid z) = \sum_{k=1}^{K} \pi_k p(x \mid \mu_k, \Sigma_k) \quad (26)$$

The "posterior probability" on a mixture component for a certain data vector is a significant derived quantity by Equation (27).

$$\gamma(z_k) \equiv p(z_k = 1 \mid x) = \frac{p(z_k=1)p(x \mid z_k=1)}{\sum_{j=1}^{K} p(z_j=1)p(x \mid z_j=1)} = \frac{\pi_k p(x \mid \mu_k, \Sigma_k)}{\sum_{j=1}^{K} \pi_j p(x \mid \mu_j, \Sigma_j)} \quad (27)$$

To maximize the Q value (s, a) in order to maximize the overall cumulative benefit, we select the action that corresponds to the highest Q value. The argmax(Q) function is used to find the action with the largest probability prediction class. The deep Q network (DQN) is utilized to estimate the function for $Qt(a)$. It employs 3x3 kernels with a stride of 2 and padding, resulting in the same filter sizes as before. $Q(s, a)$ represents the value function for action a in state S, and is updated using a learning rate of 0.01 and batch size of 16 with mean squared error. The DQN loss is calculated as the difference between the output Q values (QDQN) and the target Q values (Q target). The output Q values are computed through a forward pass: $Q(t)$DQN = FDQN(st) of the DQN. To ensure that the QDQN is as universally applicable as possible, batches of transitions of size n batch are randomly selected from the replay memory T during DQN training. This allows for extensive and evenly distributed sampling of states and surroundings. The testing is conducted for 300 episodes, each consisting of five consecutive steps, starting from a randomly selected initial state.

3.4. Performance analysis

The recommended approach is executed on a Windows 10 center i7-4710MQ computer chip running at 2.5 GHz (8 central processors), with 8 GB of Slam and 1 GB of committed illustrations handling unit memory. All experiments are performed on a personal computer with Intel Core i5 GH z processor and 8.00 GB RAM, Nvidia. The proposed method is implemented in Python 3.6.5.

The confusion matrix was analyzed in terms of true and false positives and negatives. Accuracy was calculated by dividing the total number of correct predictions (true positives + true negatives) by the total number of samples (positives + negatives). The dice score was used to measure the number of true positives as well as false positives.

$$Accuracy = \frac{(TP+TN)}{(TP+FP+TN+FN)},\ Precision = \frac{(TP)}{(TP+FP)},\ Recall = \frac{(TP)}{(TP+FN)},$$
$$DSC = 2\frac{|X \cap Y|}{|X|+|Y|} = \frac{2TP}{2TP+FN+FP} = 2\frac{Precision \times Recall}{Precision+Recall}.$$

The performance was evaluated by randomized method of "train and test" approach. The classification results for the training and test data sets are evaluated by confusion matrix in Figure 4 (a) and (b). This shows the actual and predicted class for detection of epilepsy for training and test dataset. Based on this confusion matrix, the precision recall curve is obtained by training and testing dataset for this actual and predicted class of epilepsy detection as shown in Figure 5 has the convergence of fitness over iteration, Figure 6 has training and testing accuracy and loss, Figure 7 explains confusion

Table 2
Proposed analysis based on training and testing dataset

Metrics	Training results in %	Testing results in %
Accuracy	97.39	97.04
Precision	94.81	94.12
Dice coefficient	2.61	2.96
AUC	99.52	99.56

Figure 5
Convergence of fitness over 25-iteration and 5-KCCA agents

Figure 6
Training and testing accuracy and loss

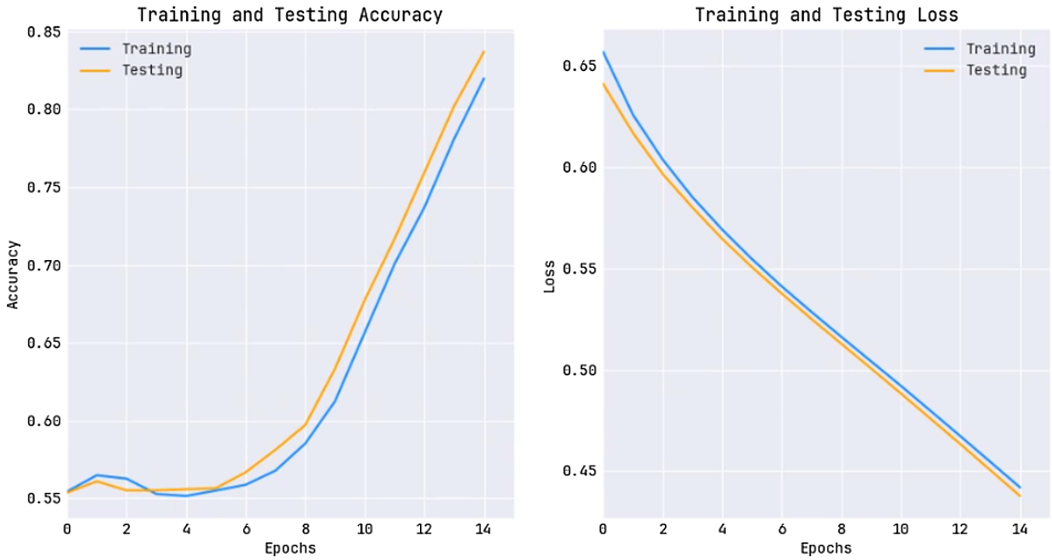

Figure 7
Confusion matrix

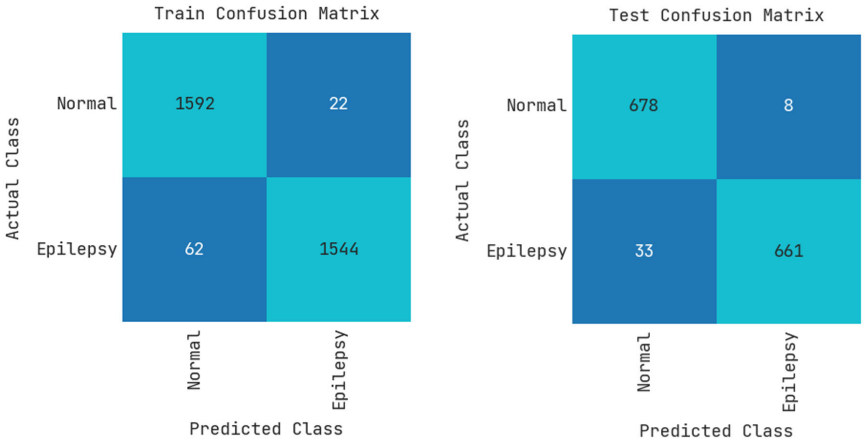

matrix, and Figures 8 and 9 show the ROC and PR curve is analyzed based on this confusion matrix.

The above Table 2 shows training and testing dataset based on proposed analysis in terms of accuracy. Accuracy is used to evaluate the overall performance by classified instances out of the total instances. A higher accuracy gives better model performance, and dice coefficient gives the similarity between two set of data (0 or 1). A higher precision value gives a low false positive rate. AUC assessed by binary classification method.

The Precision, Dice coefficient, AUC: Here, the proposed technique attained accuracy of 97.39%, precision of 94.81%, dice coefficient of 2.61, and AUC of 99.52% for training dataset; for testing dataset, proposed technique with different classifier models has attained accuracy of 97.04%, precision of 94.12%, dice coefficient of 2.96%, and AUC of 99.56% as shown in Figures 10 and 11.

Table 3 shows analysis based on training and testing dataset. Existing techniques compared are SVM, DBM, KNN, RF, and DNN with proposed model. Proposed technique attained accuracy of 97.04%, precision of 94.12%, dice coefficient of 2.96%, and AUC of 99.56%.

Recent studies have demonstrated the effectiveness of utilizing deep feature maps from convolutional neural networks for anomaly detection in EEG signals. By combining these feature maps with shallow classifiers and implementing dimensionality reduction through PCA, researchers have successfully identified preictal and interictal segments in epilepsy patients. This approach eliminates the need for manual feature extraction and has shown promising results, achieving a sensitivity of 82% and a low false prediction rate of 0.19 on epilepsy datasets. Furthermore, a deep learning system has been developed to automatically detect and differentiate spontaneous seizures in EEG data.

Table 3
Comparative analysis based on existing and proposed analysis

Metrics	SVM	DBM	KNN	RF	DNN	Proposed-KA-U-TRGN
Accuracy	86.34	87.77	90.23	93.45	95.21	97.04
Precision	84.12	83.56	88.78	91.91	93.84	94.12
Dice coefficient	10.2	9.12	7.32	4.86	4.23	2.96
AUC	91.89	93.22	96.83	97.45	98.43	99.56

Figure 8
ROC curve

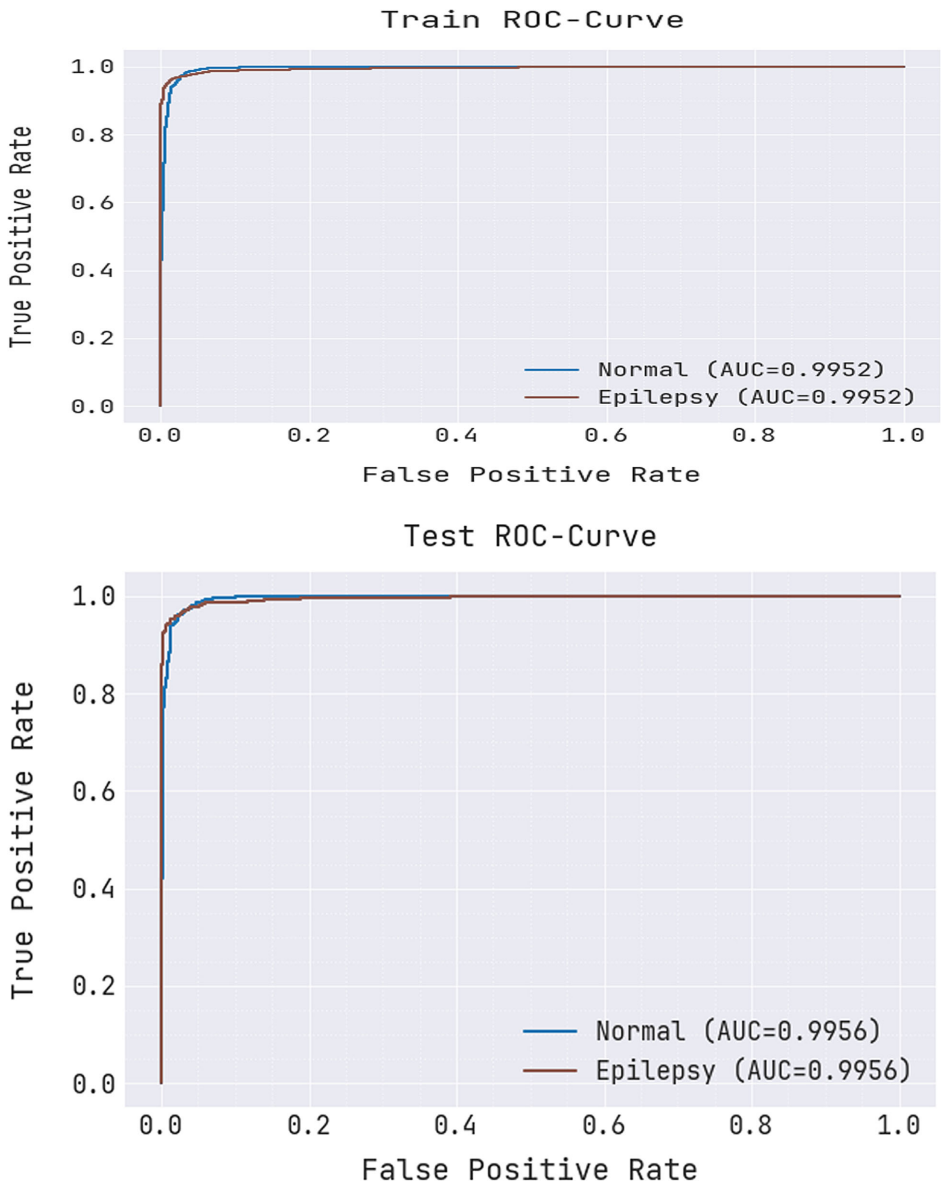

By recognizing biologically meaningful features in the data, this system achieves high performance and interpretability. Additionally, a deep network model based on ResNet theory and LSTM has been successful in classifying seizure types from EEG trials, outperforming other models with an impressive F1-score of 97.4%. Moreover, AI and IoT-based approaches have been explored for seizure detection, highlighting emerging opportunities and future research directions in this area. A comprehensive overview of different modalities for seizure detection, along with discussions on the detection processes and a novel UTRGN deep learning model enhancing performance, has been

Figure 9
PR curve of epilepsy

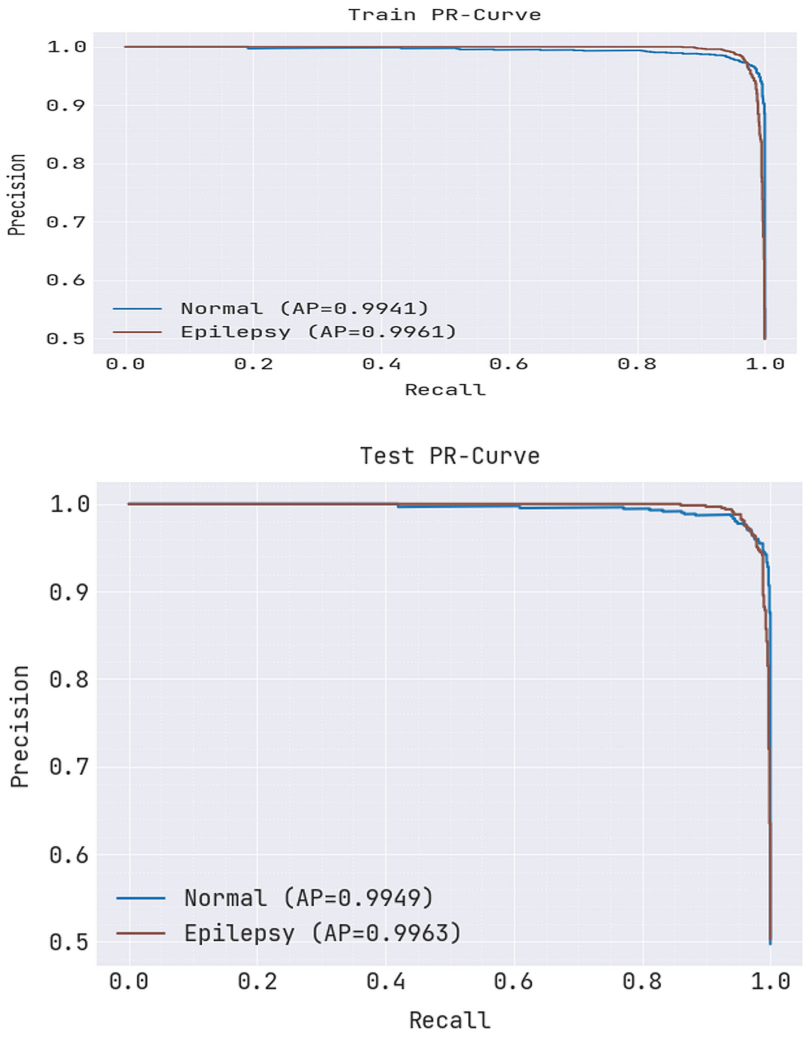

Figure 10
Comparison graph on different classifiers models

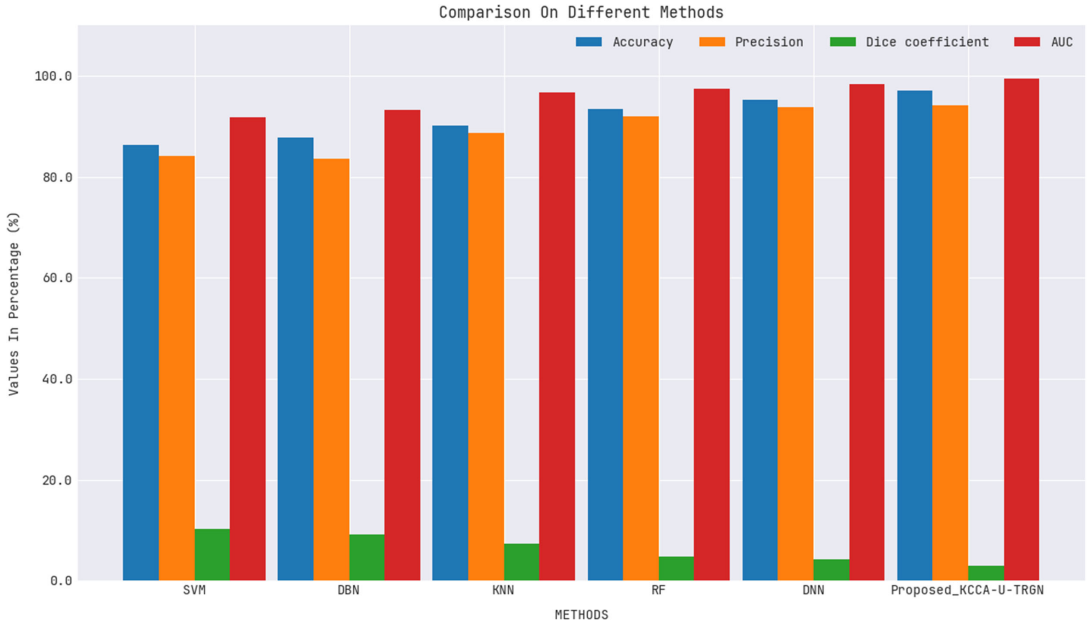

Figure 11
Comparison graph on different performance levels

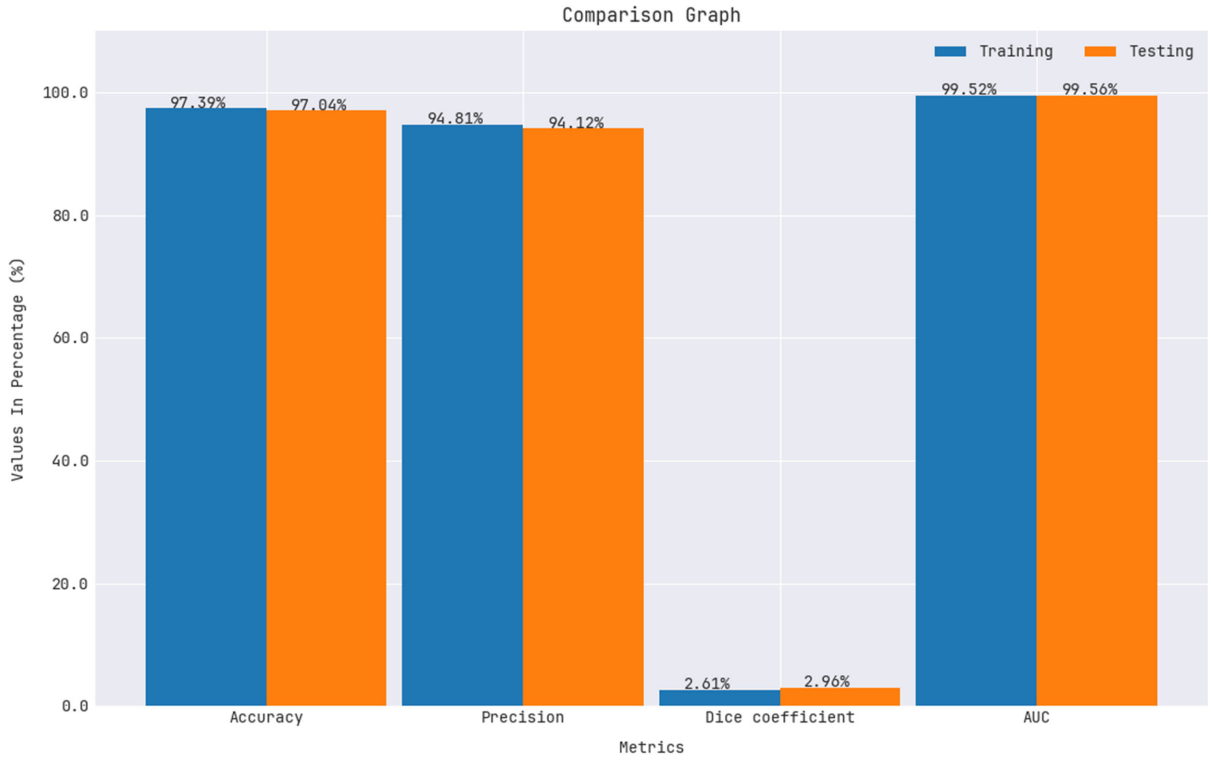

presented in recent research. Additionally, classification models such as RF and MLP have been shown to achieve high accuracies of 97 [42–47].

4. Conclusion

The proposed technique in epilepsy detection aids in selecting the processed brain signal using kernel convolutional component analysis (KCA) and the selected features are classified using UU-TRGN. Choosing the most relevant clinical variables could improve classifier performance and reduce dimensionality in small sample with specific characteristics, through the elimination of irrelevant features to increase the performance. These selected features are likely influenced by the decision to undergo surgery, with reduced predictor variables. In the combination of PET and X-ray features, the indicator variables offer limited information about the temporal areas of hypometabolism. The precise physical locations of excisions within the hippocampus, amygdala piriform cortex complex, and entorhinal cortex have been found to have a significant correlation with seizure outcomes. If these areas are targeted for surgical intervention, there is a noticeable impact on reducing epileptic seizures. AI models are used to identify specific anatomical brain regions in order to optimize surgical strategies and enhance patient outcomes.

Conflicts of Interest

The authors declare that they have no conflicts of interest to this work.

Data Availability Statement

The data that support the findings of this study are openly available in Kaggle at https://www.kaggle.com/datasets/yasserhessein/epileptic-seizure-recognition and in the UCI Machine Learning Repository at https://archive.ics.uci.edu/dataset/388/epileptic+seizure+recognition.

References

[1] Chang, A. J., Roth, R., Bougioukli, E., Ruber, T., Keller, S. S., Drane, D. L., . . . , & Alzheimer's Disease Neuroimaging Initiative. (2023). MRI-based deep learning can discriminate between temporal lobe epilepsy, Alzheimer's disease, and healthy controls. *Communications Medicine*, *3*(1), 33. https://doi.org/10.1038/s43856-023-00262-4

[2] Kang, J. Y., Wu, C., Tracy, J., Lorenzo, M., Evans, J., Nei, M., . . . , & Sperling, M. R. (2016). Laser interstitial thermal therapy for medically intractable mesial temporal lobe epilepsy. *Epilepsia*, *57*(2), 325–334. https://doi.org/10.1111/epi.13284

[3] Sakashita, K., Akiyama, Y., Hirano, T., Sasagawa, A., Arihara, M., Kuribara, T., . . . , & Mikuni, N. (2023). Deep learning for the diagnosis of mesial temporal lobe epilepsy. *PLOS ONE*, *18*(2), e0282082. https://doi.org/10.1371/journal.pone.0282082

[4] Sinclair, B., Cahill, V., Seah, J., Kitchen, A., Vivash, L. E., Chen, Z., . . . , & O'Brien, T. J. (2022). Machine learning approaches for imaging-based prognostication of the outcome of

surgery for mesial temporal lobe epilepsy. *Epilepsia*, *63*(5), 1081–1092. https://doi.org/10.1111/epi.17217

[5] Garcia-Ramos, C., Nair, V., Maganti, R., Mathis, J., Conant, L. L., Prabhakaran, V., . . . , & Struck, A. F. (2022). Network phenotypes and their clinical significance in temporal lobe epilepsy using machine learning applications to morphological and functional graph theory metrics. *Scientific Reports*, *12*(1), 14407. https://doi.org/10.1038/s41598-022-18495-z

[6] Akrami, H., Leahy, R. M., Irimia, A., Kim, P. E., Heck, C. N., & Joshi, A. A. (2022). Neuroanatomic markers of posttraumatic epilepsy based on MR imaging and machine learning. *American Journal of Neuroradiology*, *43*(3), 347–353. https://doi.org/10.3174/ajnr.A7436

[7] Meng, X., Deng, K., Huang, B., Lin, X., Wu, Y., Tao, W., . . . , & Chen, F. (2023). Classification of temporal lobe epilepsy based on neuropsychological tests and exploration of its underlying neurobiology. *Frontiers in Human Neuroscience*, *17*, 1100683. https://doi.org/10.3389/fnhum.2023.1100683

[8] Sayed, N. M., Aldin, M. T. K., Ali, S. E., & Hendi, A. E. (2023). Cognitive functions and epilepsy-related characteristics in patients with generalized tonic-clonic epilepsy: A cross-sectional study. *Middle East Current Psychiatry*, *30*(1), 15. https://doi.org/10.1186/s43045-023-00293-6

[9] Aronica, E. (2015). Gliomas and epilepsy: Insights from neuropathological studies in humans. *SpringerPlus*, *4*, L9. https://doi.org/10.1186/2193-1801-4-S1-L9

[10] Elbeh, K. A., Elserogy, Y. M., Hamid, M. F., & Gabra, R. H. (2021). Personality traits in patients with refractory versus non-refractory epilepsy. *Middle East Current Psychiatry*, *28*(1), 27. https://doi.org/10.1186/s43045-021-00106-8

[11] Al-Malt, A. M., Abo Hammar, S. A., Rashed, K. H., & Ragab, O. A. (2020). The effect of nocturnal epileptic seizures on cognitive functions in children with idiopathic epilepsy. *The Egyptian Journal of Neurology, Psychiatry and Neurosurgery*, *56*(1), 49. https://doi.org/10.1186/s41983-020-00182-3

[12] Güvenç, C., Dupont, P., van den Stock, J., Seynaeve, L., Porke, K., Dries, E., . . . , & van Paesschen, W. (2018). Correlation of neuropsychological and metabolic changes after epilepsy surgery in patients with left mesial temporal lobe epilepsy with hippocampal sclerosis. *EJNMMI Research*, *8*(1), 31. https://doi.org/10.1186/s13550-018-0385-5

[13] Abdelgawad, E. A., Mounir, S. M., Abdelhay, M. M., & Ameen, M. A. (2021). Magnetic resonance imaging (MRI) volumetry in children with nonlesional epilepsy, does it help? *Egyptian Journal of Radiology and Nuclear Medicine*, *52*(1), 35. https://doi.org/10.1186/s43055-021-00409-0

[14] Faheem, M. H., Dabour, A. S., & Abdelhaie, O. M. (2020). Diagnostic and prognostic role of proton single-voxel spectroscopy (SVS) in non-lesional epilepsy pediatric patients: Prospective controlled study. *Egyptian Journal of Radiology and Nuclear Medicine*, *51*(1), 143. https://doi.org/10.1186/s43055-020-00251-w

[15] Luckett, P. H., Maccotta, L., Lee, J. J., Park, K. Y., Dosenbach, N. U. F., Ances, B. M., . . . , & Leuthardt, E. C. (2022). Deep learning resting state functional magnetic resonance imaging lateralization of temporal lobe epilepsy. *Epilepsia*, *63*(6), 1542–1552. https://doi.org/10.1111/epi.17233

[16] Wang, J., Guo, K., Cui, B., Hou, Y., Zhao, G., & Lu, J. (2022). Individual [^{18}F] FDG PET and functional MRI based on simultaneous PET/MRI may predict seizure recurrence after temporal lobe epilepsy surgery. *European Radiology*, *32*(6), 3880–3888. https://doi.org/10.1007/s00330-021-08490-9

[17] Qu, R., Wang, S., Liu, Z., Gu, J., & Xu, G. (2022). 3D-CNN frameworks for mesial temporal lobe epilepsy diagnosis in MRI images. *International Journal of Applied Electromagnetics and Mechanics*, *70*(4), 515–523. https://doi.org/10.3233/JAE-220003

[18] Vorndran, J., Neuner, C., Coras, R., Hoffmann, L., Geffers, S., Honke, J., . . . , & Jabari, S. (2023). A deep learning-based histopathology classifier for Focal Cortical Dysplasia. *Neural Computing and Applications*, *35*(17), 12775–12792. https://doi.org/10.1007/s00521-023-08364-9

[19] Pisano, B., Teixeira, C. A., Dourado, A., & Fanni, A. (2020). Application of self-organizing map to identify nocturnal epileptic seizures. *Neural Computing and Applications*, *32*(24), 18225–18241. https://doi.org/10.1007/s00521-019-04327-1

[20] Raab, D., Theissler, A., & Spiliopoulou, M. (2023). XAI4EEG: Spectral and spatio-temporal explanation of deep learning-based seizure detection in EEG time series. *Neural Computing and Applications*, *35*(14), 10051–10068. https://doi.org/10.1007/s00521-022-07809-x

[21] Raghu, S., Sriraam, N., Vasudeva Rao, S., Hegde, A. S., & Kubben, P. L. (2020). Automated detection of epileptic seizures using successive decomposition index and support vector machine classifier in long-term EEG. *Neural Computing and Applications*, *32*(13), 8965–8984. https://doi.org/10.1007/s00521-019-04389-1

[22] Glory, H. A., Vigneswaran, C., Jagtap, S. S., Shruthi, R., Hariharan, G., & Sriram, V. S. (2021). AHW-BGOA-DNN: A novel deep learning model for epileptic seizure detection. *Neural Computing and Applications*, *33*(11), 6065–6093. https://doi.org/10.1007/s00521-020-05384-7

[23] Mendonça, F., Fred, A., Mostafa, S. S., Morgado-Dias, F., & Ravelo-García, A. G. (2022). Automatic detection of cyclic alternating pattern. *Neural Computing and Applications*, *34*(13), 11097–11107. https://doi.org/10.1007/s00521-018-3474-5

[24] Dang, N., Shao, K., Chen, L., & Yang, M. (2022). Multi-model decision-making seizure types classification based on transfer learning. In *International Symposium on Control Engineering and Robotics*, 192–201. https://doi.org/10.1109/ISCER55570.2022.00040

[25] Siddiqui, M. K., Islam, M. Z., & Kabir, M. A. (2019). A novel quick seizure detection and localization through brain data mining on ECoG dataset. *Neural Computing and Applications*, *31*(9), 5595–5608. https://doi.org/10.1007/s00521-018-3381-9

[26] Kang, L., Chen, J., Huang, J., Zhang, T., & Xu, J. (2022). Identifying epilepsy based on machine-learning technique with diffusion kurtosis tensor. *CNS Neuroscience & Therapeutics*, *28*(3), 354–363. https://doi.org/10.1111/cns.13773

[27] Zhang, Y., Zhang, D., Chen, Z., Wang, H., Miao, W., & Zhu, W. (2022). Clinical evaluation of a novel atlas-based PET/CT brain image segmentation and quantification method for epilepsy. *Quantitative Imaging in Medicine and Surgery*, *12*(9), 4538–4548. https://doi.org/10.21037/qims-21-1005

[28] Ahmad, I., Wang, X., Zhu, M., Wang, C., Pi, Y., Khan, J. A., . . . , & Li, G. (2022). [Retracted] EEG-Based Epileptic Seizure Detection via Machine/Deep Learning Approaches: A Systematic Review. *Computational Intelligence and Neuroscience*, *2022*(1), 6486570. https://doi.org/10.1155/2022/6486570

[29] Debicki, D. B. (2017). Electroencephalography after a single unprovoked seizure. *Seizure*, *49*, 69–73. https://doi.org/10.1016/j.seizure.2017.03.001

[30] Miltiadous, A., Tzimourta, K. D., Giannakeas, N., Tsipouras, M. G., Glavas, E., Kalafatakis, K., & Tzallas, A. T. (2023). Machine learning algorithms for epilepsy detection based

on published EEG databases: A systematic review. *IEEE Access*, *11*, 564–594. https://doi.org/10.1109/ACCESS.2022.3232563

[31] Xiong, Z., Wang, H., Zhang, L., Fan, T., Shen, J., Zhao, Y., . . . , & Wu, Q. (2021). A study on seizure detection of EEG signals represented in 2D. *Sensors*, *21*(15), 5145. https://doi.org/10.3390/s21155145

[32] Alotaibi, S. M., Rahman, A., Basheer, M. I., & Khan, M. A. (2021). Ensemble machine learning based identification of pediatric epilepsy. *Computers, Materials & Continua*, *68*(1), 149–165.

[33] Bayrak, S., Yucel, E., & Takci, H. (2022). Epilepsy radiology reports classification using deep learning networks. *Computers, Materials & Continua*, *70*(2), 3589–3607.

[34] Beatrice, S., & Meena, J. (2022). Overhauled approach to effectuate the amelioration in EEG analysis. *Intelligent Automation & Soft Computing*, *33*(1), 331–347.

[35] Cheng, Z., Tao, Y., Gu, X., Jiang, Y., & Qian, P. (2023). Cross-domain TSK fuzzy system based on semi-supervised learning for epilepsy classification. *Computer Modeling in Engineering & Sciences*, *137*(2), 1613–1633.

[36] Cherukuvada, S., & Kayalvizhi, R. (2023). Feature selection with deep belief network for epileptic seizure detection on EEG signals. *Computers, Materials & Continua*, *75*(2), 4101–4118.

[37] Hu, J., Mo, J., & Cheng, X. (2023). Microglial TRPV1 in epilepsy: Is it druggable for new antiepileptic treatment? *BIOCELL*, *47*(8), 1689–1701.

[38] Liu, J., Du, Y., Wang, X., Yue, W., & Feng, J. (2022). Automated machine learning for epileptic seizure detection based on EEG signals. *Computers, Materials & Continua*, *73*(1), 1995–2011.

[39] Naseem, S., Javed, K., Khan, M. J., Rubab, S., Khan, M. A., & Nam, Y. (2021). Integrated CWT-CNN for epilepsy detection using multiclass EEG dataset. *Computers, Materials & Continua*, *69*(1), 471–486.

[40] Wang, J. Q., Fang, W., & Sheng, V. S. (2022). Prediction of epileptic EEG signal based on SECNN-LSTM. *Journal of New Media*, *4*(2), 73–84.

[41] Wang, J., Li, B., Qiu, C., Zhang, X., Cheng, Y., Wang, P., . . . , & Cai, J. (2023). Multi-view & transfer learning for epilepsy recognition based on EEG signals. *Computers, Materials & Continua*, *75*(3), 4843–4866.

[42] Alalayah, K. M., Senan, E. M., Atlam, H. F., Ahmed, I. A., & Shatnawi, H. S. A. (2023). Effective early detection of epileptic seizures through EEG signals using classification algorithms based on t-distributed stochastic neighbor embedding and K-means. *Diagnostics*, *13*(11), 1957. https://doi.org/10.3390/diagnostics13111957

[43] Alshaya, H., & Hussain, M. (2023). EEG-based classification of epileptic seizure types using deep network model. *Mathematics*, *11*(10), 2286. https://doi.org/10.3390/math11102286

[44] Ein Shoka, A. A., Dessouky, M. M., El-Sayed, A., & Hemdan, E. E. D. (2023). EEG seizure detection: Concepts, techniques, challenges, and future trends. *Multimedia Tools and Applications*, *82*(27), 42021–42051. https://doi.org/10.1007/s11042-023-15052-2

[45] Ibrahim, A. K., Zhuang, H., Tognoli, E., Muhamed Ali, A., & Erdol, N. (2023). Epileptic seizure prediction based on multiresolution convolutional neural networks. *Frontiers in Signal Processing*, *3*, 1175305. https://doi.org/10.3389/frsip.2023.1175305

[46] Statsenko, Y., Babushkin, V., Talako, T., Kurbatova, T., Smetanina, D., Simiyu, G. L., . . . , & Ljubisavljevic, M. (2023). Automatic detection and classification of epileptic seizures from EEG data: Finding optimal acquisition settings and testing interpretable machine learning approach. *Biomedicines*, *11*(9), 2370. https://doi.org/10.3390/biomedicines11092370

[47] Zeng, W., Shan, L., Su, B., & Du, S. (2023). Epileptic seizure detection with deep EEG features by convolutional neural network and shallow classifiers. *Frontiers in Neuroscience*, *17*, 1145526. https://doi.org/10.3389/fnins.2023.1145526

How to Cite: Vajiram, J., S., S., Jena, R., & Maurya, U. (2024). Epilepsy Detection by Different Modalities with the Use of AI-Assisted Models. *Artificial Intelligence and Applications*, *2*(3), 204–217. https://doi.org/10.47852/bonviewAIA32021848